Ultra-fast intensified frame images from an electron cyclotron resonance hydrogen plasma at 2.45 GHz: Some space distributions of visible and monochromatic emissions[a)]

O. D. Cortázar,[1,b)] A. Megía-Macías,[2] A. Vizcaíno-de-Julián,[2] O. Tarvainen,[3] J. Komppula,[3] and H. Koivisto[3]
[1]*Universidad de Castilla-La Mancha, ETSII - INEI, C.J. Cela s/n, 13170 Ciudad Real, Spain*
[2]*E.S.S. Bilbao, Edificio Cosimet, Landabarri 2, 48940-Leioa, Vizcaya, Spain*
[3]*Department of Physics, Accelerator Laboratory, University of Jyväskylä, PO Box 35 (YFL), 40500 Jyväskylä, Finland*

(Presented 12 September 2013; received 2 September 2013; accepted 19 September 2013; published online 16 October 2013)

First results from an ultra-fast frame image acquisition diagnostic coupled to a 2.45 GHz microwave hydrogen discharge are presented. The plasma reactor has been modified to include a transparent doubled shielded quartz window allowing to viewing the full plasma volume. Pictures describing the breakdown process at 1 μs exposure time have been obtained for integrated visible light signal, Balmer-alpha, Balmer-beta lines, and Fulcher-band. Several different plasma emission distributions are reported. The distribution depends on the magnetic field configuration, incident microwave power, and neutral gas pressure. © *2013 AIP Publishing LLC*. [http://dx.doi.org/10.1063/1.4824812]

I. INTRODUCTION

High temporal resolution images in visible light range have been an important diagnostics tool for plasma physics research and its applications during the past decades. Such imaging yields information about the spatial distribution of electrons as well as ionization and molecular dissociation processes. However, only a few studies probing the spatial and/or temporal light emission profiles of ECR-heated plasmas have been conducted.[1–3] Herein we present initial results measured with a pulsed 2.45 GHz hydrogen plasma generator coupled with bandpass filters and Image Intensified CCD frame camera, which is based on a combination of multichannel plate (MCP) light intensifiers and CCD cameras.

II. THE ECR 2.45 GHz ION SOURCE PLASMA GENERATOR

The 2.45 GHz plasma generator, driven by a 3 kW adjustable power magnetron operated in pulsed mode at 50 Hz, is similar to modern microwave ion sources intended for the production of intense proton beams. A detailed description of the device can be found from Refs. 4 and 5. The main parts of the device are listed in the caption of Fig. 1. The figure also shows the modification required for this work, i.e., an optically transparent window allowing to view the full plasma volume. Two grids of 2.5 mm square structure made of 0.25 mm tungsten wires and grounded to the plasma chamber are placed at both sides of the 10 mm thick quartz window that has a cylindrical hole with 7 mm diameter at its center. Such design meets three important criteria: (a) to obtain an image covering the whole plasma chamber volume, (b) to pump gas trough the axial hole, and (c) prevent microwave losses through the quartz window as confirmed by the measurement of non-ionizing radiation with a specific radiometric device by NARDA, mod. NBM-550. No significant performance differences have been observed between the modified plasma generator and the original one with aluminum plasma electrode.

III. DIAGNOSTICS SETUP

Figure 2 shows the schematics of the experimental setup and timing system. Images are acquired with an Intensified Frame CCD Camera System made by Cordin Corp. (model 220A). A Pentax 67 × 150 mm telephoto lens with a focus ring to reduce the minimum focus distance is attached to the camera. The setup enables taking up to four images with independently adjusted exposure times and delays between each shot. Typical exposure time used in this study is 1 μs while the delay between frames depends on the plasma dynamics specific to the plasma generator settings. The MCP and CCD gains can be adjusted depending on the light intensity to optimize the images taken through different filters at various stages of the microwave pulse. It is of note that the independent settings of the MCPs and CCDs make it necessary to perform a calibration in order to compare the images. The images are transformed through the calibration into a representation where red corresponds to highest intensity (saturated white on black and white gamma) and blue the lowest (deep black). The auxiliary diagnostics include the measurement of incident and reflected power signals recorded by bidirectional couplers. The time-resolved light emission is also obtained through an optical fiber placed at the periphery of the optical window and connected to a fast photodiode. The setup allows mounting bandpass filters in front of the CCD camera

[a)]Contributed paper, published as part of the Proceedings of the 15th International Conference on Ion Sources, Chiba, Japan, September 2013.
[b)]Electronic mail: dcortazar@essbilbao.org.

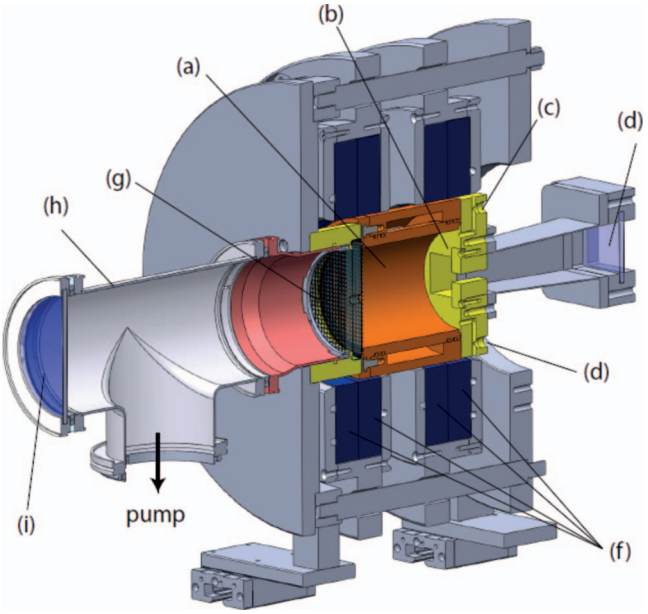

FIG. 1. A cross sectional view of the plasma reactor: (a) plasma chamber, (b) microwave coupler, (c) gas inlet, (d) RF quartz window, (f) coil pancakes, (g) optical window with shielding grids, (h) vacuum tee, and (i) standard quartz window placed in front of the camera.

and the photodiode in order to study (nearly) monochromatic light emission in visible light range.

IV. RESULTS

The main purpose of this report is to demonstrate the temporal capabilities of the diagnostics setup and discuss the interpretation of the images. Therefore, only representative examples of the measurement results are presented in this section. Figure 3 shows a set of pictures taken at different stages of the breakdown process of a hydrogen discharge for Visible emission range (390–700 nm), Balmer-alfa (656.3 nm), Balmer-beta (486.1 nm), and Fulcher band (around 600 nm) by using bandpass filters (Thorlabs models FB660-10, FL488-10, and FB600-40). The corresponding operational parameters are 2100 W incident power and 1200 W of reflected power at 50 Hz/10% duty factor, 3.8×10^{-3} mbar neutral gas pressure and $B \simeq ECR/2$ magnetic field (0.044 T on axis). The set of pictures is divided into two groups separated by a dashed vertical line. The group on the left is obtained at the very beginning of the plasma breakdown when the corresponding intensity of light emission is relatively low. The second set of pictures on the right is obtained at later stage of the discharge when the light intensity is significantly higher. Thus, the two groups of pictures have been measured on different pulses using different MCP gains avoiding overexposure. This fact prohibits comparing the intensities of the false color images between the groups.

Three observations can be made: (a) it takes only some tens of μs to reach the light emission profile (prevailing through the microwave pulse), (b) the light emission profile is similar for atomic (Balmer lines) and molecular emission (Fulcher band), and (c) the light emission profile is not homogeneous but instead is prolonged along the direction of the microwave electric field polarization. Following the plasma breakdown, the atomic and molecular emission intensities always follow opposing trends. The atomic emission intensity increases while molecular emission intensity decreases towards the end of the pulse. Figure 4 where normalized photodiode signals are shown for the full microwave pulse is a representative example recorded with experimental parameters listed above for Fig. 3. It is important to note that the

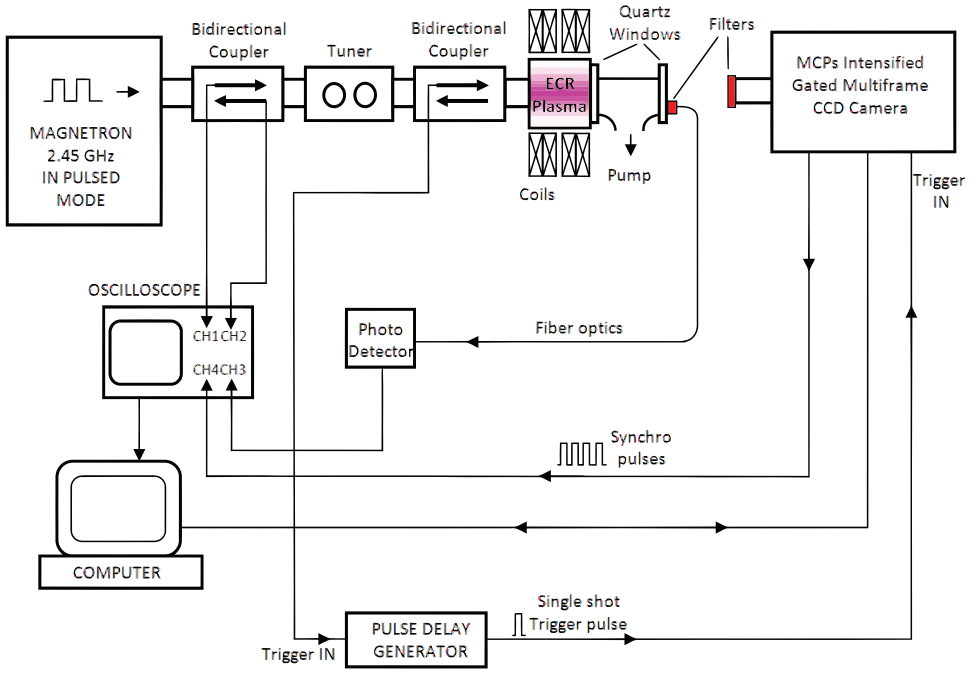

FIG. 2. Schematic presentation of the experimental setup.

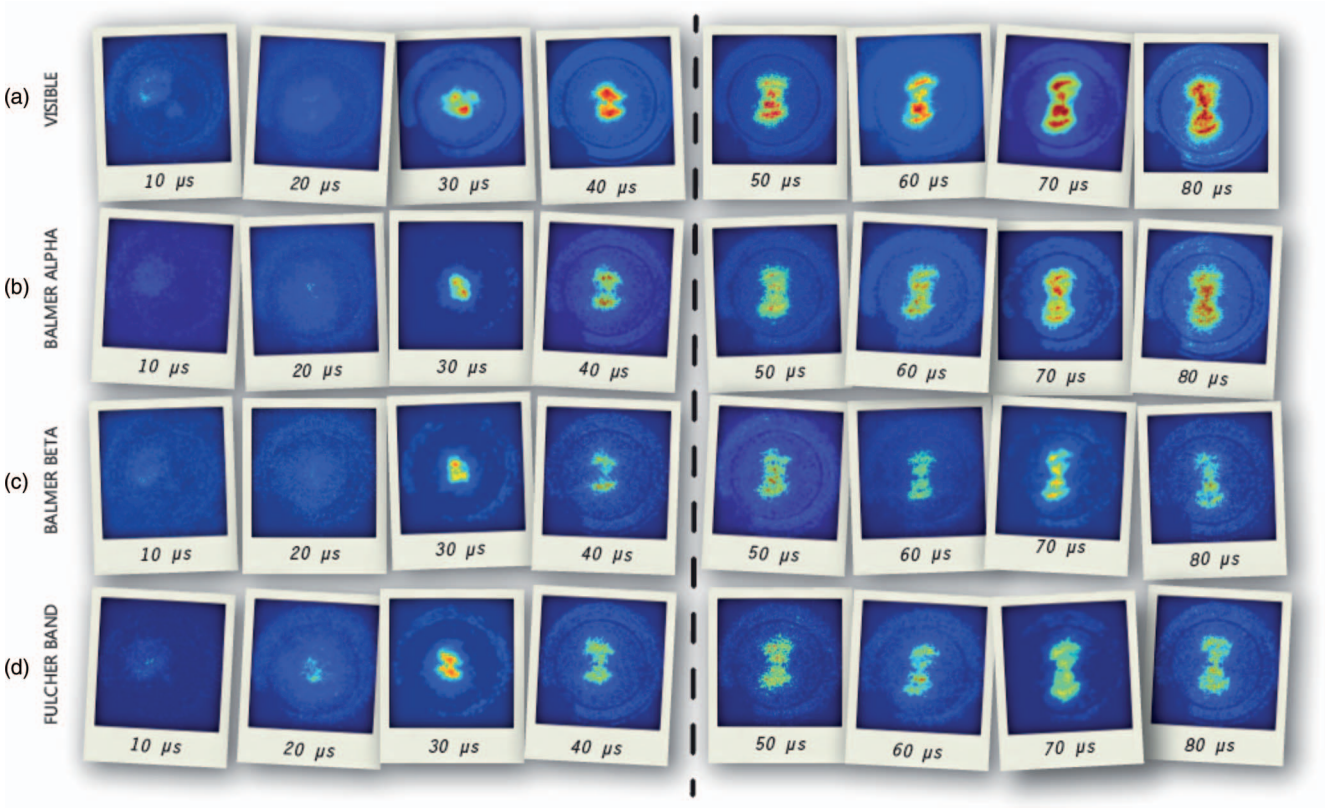

FIG. 3. Typical example of normalized CCD images of visible light (390–700 nm) (a), Balmer-alpha (656.3 nm) (b), Balmer-beta (486.1 nm) (c), and Fulcher-band (around 600 nm) (d) taken at different stages of the plasma breakdown. The given times are measured from the leading edge of the microwave pulse.

spatial distribution of the light emission depends strongly on the experimental conditions. Figure 5 shows various visible light distributions and their evolution during the plasma breakdown. These distributions represent all cases observed during the experiments and they have been named according to their visual appearances, i.e., *Butterfly*, *Homogeneous*, *Ring*, and *Column*. It is of note that there are significant differences between the evolution times, ranging from less than 10 μs to more than 50 μs, of the given profiles during the breakdown process.

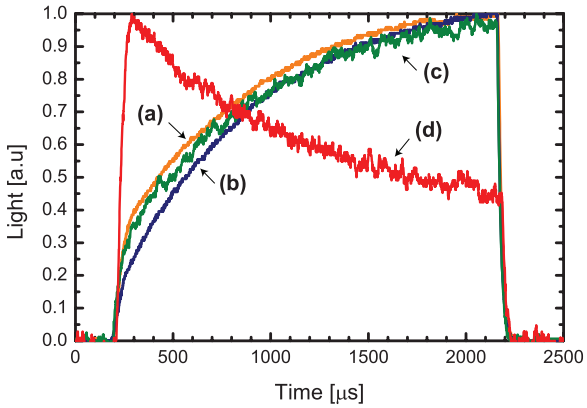

FIG. 4. Normalized photodiode signals corresponding to visible light (390–700 nm) (a), Balmer-alpha (656.3 nm) (b), Balmer-beta (486.1 nm) (c), and Fulcher-band (around 600 nm) (d). The temporal scale has been shifted by 200 μs for visual reasons.

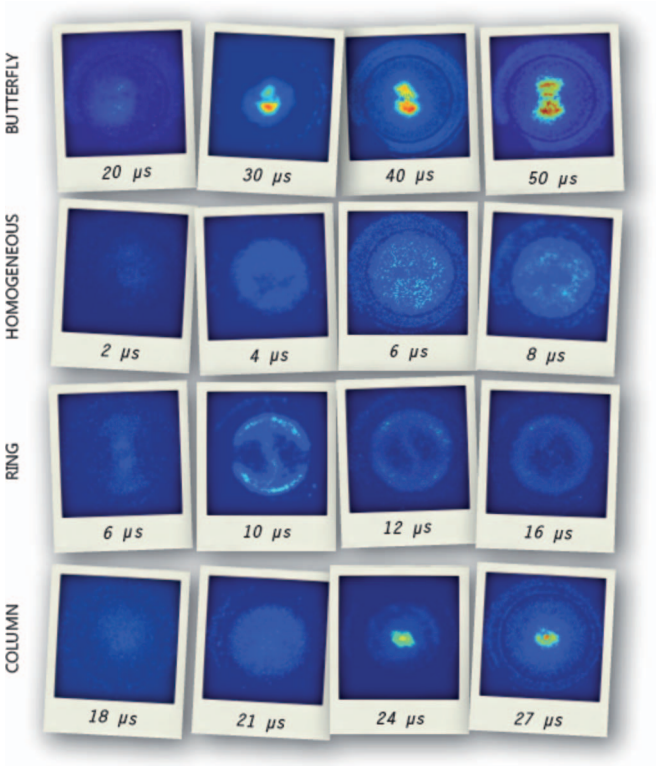

FIG. 5. Examples of visible light emission distributions observed under different experimental conditions during the plasma breakdown. *Butterfly* shape was obtained at $B \simeq ECR/2$, *Column* shape at $B \simeq ECR$ and *Homogeneous* and *Ring* at $B > ECR$. All cases were recorded with a neutral gas pressure of 1.6×10^{-3} mb.

V. DISCUSSION AND CONCLUSION

In order to interpret the results and discuss their implications it is important to keep in mind the basic underlying processes resulting to visible light emission from the hydrogen plasma, i.e., the excitation of neutral hydrogen atoms and molecules by electron impact from level q to level p and the decay into level k by spontaneous emission resulting in line emission pk. The hydrogen Balmer series corresponds to the transitions from the excited states of atomic hydrogen with the primary quantum number $n_p > 2$ to the excited state with $n_k = 2$. Balmer-alpha radiation at 656.3 nm is emitted when $n_p = 3$, i.e., it is the primary transition within the Balmer-series. For Balmer-beta the corresponding numbers are 486.1 nm and $n_p = 4$. The $n = 3$ and $n = 4$ states are populated by atomic excitation and dissociative excitation of H_2 - molecules by electron impact. The relative importance of these processes depends on the densities of neutral atoms and molecules as well as the distribution of electron energies. In low temperature plasmas (Te on the order of 10 eV) the rate for atomic excitation is typically greater by more than an order of magnitude.[6] However, the exact ratio of the two excitation channels depends on the vibrational distribution of the molecules. The Fulcher-band emission around 600 nm corresponds to the molecular triplet transition $d^3\Pi_u \rightarrow a^3\Sigma_g^+$ with a further transition (emission in UV) $a^3\Sigma_g^+ \rightarrow b^3\Sigma_u^+$ to a repulsive state (molecular continuum, see, for example, Ref. 7). Thus, Fulcher-band emission indicates dissociation of the emitting molecule. The radiative lifetimes of the excited states resulting to light emission within the Balmer series and Fulcher-band are on the order of 10^{-7} s and 10^{-8} s, respectively.[7,8] The typical speed of the hydrogen atoms and/or molecules can be estimated from their temperature (kinetic energy). It is assumed that the maximum temperature of the neutral population is on the order of 1 eV corresponding to typical ion temperature in the plasma. This translates to rms-speed of 10^4 m/s (order of magnitude). Therefore, the maximum distance governed by the neutral particles between the collisional excitation and subsequent light emission is on the order of 10^{-3} m. In reality the energy distribution of the neutral particles is much more narrow but estimating the maximum rms-speed/distance serves the purpose in this case. The evident conclusion is that the spatial light emission profile corresponds to the spatial distribution of excitation collisions, i.e., distribution of energetic electrons and ionization. Furthermore, the distribution of Fulcher band emission indicates the spatial distribution of molecular dissociation. The atomic and molecular light emission profiles being similar suggests that the distribution the neutral species is uniform.

The fact that the light emission is not always uniform but (in some cases) follows the polarization of the microwave electric field cannot be explained unambiguously. It suggests that in some particular cases the microwave power is being absorbed only in a well-defined volume and hot electrons are not diffusing across the magnetic field lines, i.e., their mean free path is longer than the dimension of the plasma chamber. The light emission profile is sensitive to magnetic field topology and strength, neutral gas pressure, incident microwave power, and plasma-microwave coupling, i.e., impedance matching. Clear tendencies on the given parameters have not been identified so far and, hence, the topic will be studied further in the future. The microwave-plasma coupling differs remarkably between different plasma emission profiles shown in Fig. 5. Relative low reflected power (55%) indicating good coupling is typically recorded for the *Butterfly* distribution at $B \simeq ECR/2$ field and for the *Column* distribution at $B = ECR$. The two other distributions (*Homogeneous* and *Ring*) correspond to poor microwave coupling indicated by high reflected power (95%–98%, respectively) and low light intensity. The microwave-plasma coupling affects the breakdown as suggested by the data in Fig. 5.

The initial results presented in this paper demonstrate the capabilities of the diagnostics setup, which is ideal for studying the microwave-plasma coupling and physics of the discharge breakdown (decay). The photodiode coupled with Balmer-series and Fulcher-band filters is an extremely useful diagnostics for ion sources intended for proton beam production as the temporal signals of the atomic and molecular light emission could be used to determine the species fraction of the extracted beam without separation of the charged particles downstream in the beam line. Such diagnostics could significantly reduce the time required for ion source tuning and troubleshooting. Further experiments with a Wien filter to confirm this will be conducted shortly.

ACKNOWLEDGMENTS

The authors want to express their gratitude to F. J. Bermejo and J. Bordas for the continuous institutional support.

[1] R. Racz, S. Biri, and J. Palanikas, Plasma Sources Sci. Technol. **20**, 025002 (2011).
[2] G. Castro, D. Mascali, F. Romano, L. Celona, S. Gammino, D. Lanaia, R. Di-Giugno, R. Miracoli, T. Serafino, F. Di-Bartolo, N. Gambino, and G. Ciavola, Rev. Sci. Instrum. **83**, 02B501 (2012).
[3] N. Nishino, Y. Nakashima, Y. Higashizono, S. Kobashashi, K. Islam, Y. Kubota, M. Yoshikawa, Y. Mishima, and T. Cho, Plasma Fusion Res. **1**, 035 (2006).
[4] O. D. Cortázar, A. Megía-Macías, and A. Vizcaíno-de Julián, Rev. Sci. Instrum. **83**, 103302 (2012).
[5] O. D. Cortázar, J. Komppula, O. Tarvainen, A. Megía-Macías, A. Vizcaíno-de Julián, and H. Koivisto, Plasma Sources Sci. Technol. **22**, 015026 (2013).
[6] K. Behringer and U. Fantz, New J. Phys. **2**, 23 (2000).
[7] U. Fantz and D. Wűnderlich, At. Data Nucl. Data Tables **92**, 853 (2006).
[8] Y. Verolaĭnen and Y. Nikolaich, Sov. Phys. Usp. **25**, 431 (1982).